Prefrontal control over occipital responses to crossmodal overlap varies across the congruency spectrum

Johan N. Lundström[1,2,3], Christina Regenbogen[1,4,5], Kathrin Ohla[2,6], and Janina Seubert[1,2,7]

[1] Department of Clinical Neuroscience, Karolinska Institutet, Stockholm, Sweden

[2] Monell Chemical Senses Center, Philadelphia, PA, United States

[3] Department of Psychology, University of Pennsylvania, Philadelphia, United States

[4] Department of Psychiatry, Psychotherapy and Psychosomatics, Medical School, RWTH Aachen University, Germany

[5] JARA - BRAIN Institute 1: Structure-Function Relationship: Decoding the Human Brain at systemic levels, Forschungszentrum Jülich, Germany

[6] Cognitive Neuroscience, Institute of Neuroscience and Medicine (INM-3), Research Center Jülich, Jülich, Germany

[7]Aging Research Center, Department of Neurobiology, Care Sciences and Society, Karolinska Institutet and Stockholm University

Corresponding authors:

Janina Seubert, PhD
Dept. of Clinical Neuroscience
Karolinska Institutet
Nobels väg 9
17177 Stockholm, Sweden
E-mail: Janina.Seubert@ki.se

&

Johan Lundström, PhD
Dpt. of Clinical Neuroscience
Karolinska Institutet
Nobels väg 9
17177 Stockholm, Sweden
E-mail: Johan.Lundstrom@ki.se

Abstract

While matched crossmodal information is known to facilitate object recognition, it is unclear how our perceptual systems encode the more gradual congruency variations that occur in our natural environment. Combining visual objects with odor mixtures to create a gradual increase in semantic object overlap, we demonstrate high behavioral acuity to linear variations of olfactory-visual overlap in a healthy adult population. This effect was paralleled by a linear increase in cortical activation at the intersection of occipital fusiform and lingual gyri, indicating linear encoding of crossmodal semantic overlap in visual object recognition networks. Effective connectivity analyses revealed that this integration of olfactory and visual information was achieved by direct information exchange between olfactory and visual areas. In addition, a parallel pathway through the superior frontal gyrus was increasingly recruited towards the most ambiguous stimuli. These findings demonstrate that cortical structures involved in object formation are inherently crossmodal and encode sensory overlap in a linear manner. The results further demonstrate that prefrontal control of these processes is likely required for ambiguous stimulus combinations, a fact of high ecological relevance that may be inappropriately captured by common task designs juxtaposing congruency and incongruency.

Keywords: multisensory, olfaction, vision, connectivity, congruency

Introduction

Objects in our environment commonly emit signals through more than one sensory channel. The cortical integration of these multisensory signals facilitates their attribution to a common source, and thus provides the emitting object with the unique neural signature that is crucial to its successful identification (Mesulam 1998; Binkofski et al. 2004). A key operating principle for cortical multisensory signal integration is the preferential binding of stimuli that have been experienced in combination previously and are thus perceived as “familiar”, or “semantically congruent” (Laurienti et al. 2004): compared to mismatched stimuli (e.g., the sound of a cat and picture of a dog), two semantically matched stimuli (e.g., sound and picture of a dog) mutually enhance localized cortical activity in unisensory perceptual cortices, as well as in networks supporting semantic object classification such as ventral temporal lobe structures, and executive areas in prefrontal association cortex (Hein et al. 2007; van Atteveldt et al. 2014; Gau and Noppeney 2016).

The juxtaposition of completely matched versus completely mismatched stimuli, however, inadequately matches every day challenges in object perception, where perfect repetitions of stimulus combinations are rare. In real life, stimuli tend to be organized into feature categories: instead of being ideal replica of previously encountered examples of the same object type, they fall on a distance continuum relative to the center of the object category they represent (Leopold et al. 2001; Iordan et al. 2016). Mounting evidence indicates that our perceptual systems solve this continuity of object boundaries through a weighted assessment of all evidence carried by the available information (Kersten and Yuille 2003; Kersten et al. 2004; Kayser and Shams 2015; Rohe and Noppeney 2015). To what extent familiarity-based integration of multisensory overlap follows similar principles is to date poorly understood. While

an imperfect match between sensory modalities should cause a proportionally reduced congruency response at the cortical level, this has not so far explicitly been tested, and any possible cortical support networks that might contribute to the formation of such a weighted congruency response remain understudied. Perceptual decision-making tasks within single modalities that vary the object-likeness of stimuli between two object categories through linear increases in sensory noise often demonstrate increased prefrontal recruitment as the amount of noise approaches its maximum (Corbetta and Shulman 2002; Pessoa et al. 2003; Hebart et al. 2012). An increasing body of work (Seubert et al. 2015; Regenbogen et al. 2016, 2017; Ohla et al. 2017) indicates that similar mechanisms likely also mediate multisensory integration with increasing perceptual difficulty (Doehrmann and Naumer 2008). Tasks with a lower cognitive-analytical load, such as the juxtaposition of clearly incongruent and clearly congruent combinations, might be less reliant on top-down control than tasks with more complex sensory stimuli and thus fail to appropriately capture top-down control of sensory integration, despite the potentially crucial relevance of these mechanisms in more ecologically valid settings of imperfect match or mismatch. A deeper investigation of a potential non-linear recruitment of heteromodal association cortex during the formation of gradual multisensory object percepts is thus urgently warranted.

Despite their obvious ecological relevance, stimuli that represent transitions across object boundaries are notoriously difficult to manipulate with precise control in an experimental setting. In the visual and auditory modalities especially, the simultaneous variation of parameters required for morphing between different objects often results in percepts that are perceived as unnatural or unidentifiable. The olfactory modality carries a unique natural advantage in this respect: nearly all odors are natural mixtures, they are habitually merged into meaningful odor objects, and linearity can

easily be created through gradual dilution of one odorant within another (Gottfried 2010; Wilson and Sullivan 2011; Seubert et al. 2014; Amsellem and Ohla 2016). For the present study, we used such a linear mixture series between two odorants associated with specific food items together with simultaneously presented images of these target food items to experimentally implement gradual changes in semantic congruency (i.e., learned object representation) between the two sensory modalities.

The aim of this study was to investigate the ability of human subjects to form continuous perceptual representations of semantic overlap between sensory modalities, and to delineate the cortical mechanisms that underlie this ability. First, humans' sensitivity to linear modulations in semantic overlap between the olfactory mixture series and visual stimuli was established to ensure the behavioral relevance of the modulation (Behavioral Session). We then investigated the cortical mechanisms underlying these behavioral modulations using fMRI (Imaging Session). Specifically, we hypothesized that cortical areas linked to object identification would show a continuous activity increase in correspondence with the degree of crossmodal semantic overlap between olfactory and visual information. Moreover, we hypothesized that specific support structures for sensory integration could be identified in heteromodal association cortices. Finally, we hypothesized that the mediatory role of this top-down regulation would vary across the congruency spectrum in a non-linear manner; that is, that recruitment would be strongest for mixtures in the middle of the congruency spectrum, where the cognitive-analytical task load is highest.

Materials & Methods

Ethics statement

All participants provided written, informed consent prior to participation, and all aspects of the study were approved by the University of Pennsylvania's Institutional Review Board (IRB) prior to starting the study and performed in accord with the Declaration of Helsinki on Biomedical Studies Involving Human Subjects.

Behavioral assessment

Participants

Twenty individuals who reported themselves as healthy and with normal olfactory and visual (correction allowed) functions participated in the behavioral assessment portion of the study (17 women, M age = 30 years, SD = 6.5 years). Due to the poor correspondence between self-assessment and actual occurrence of olfactory dysfunction (Landis et al. 2003), an assessment of olfactory performance was conducted. All participants correctly identified 11 or more out of 16 odorants from the Sniffin' Sticks Test battery (M=14.2), indicating normal olfactory abilities (Kobal et al. 2000). None of the participants suffered from a cold or allergies that could potentially impair olfactory functioning at the time of testing.

Stimuli and stimulus delivery

Participants evaluated the perceived semantic congruency of simultaneously presented olfactory and visual stimuli. Visual stimuli consisted of photographs of oranges or peanuts (5 images for each category). Images were selected from a larger set to be maximally identifiable as exemplars of their respective category by a panel of ten independent raters. Images were cropped to exclude any contextual cues, and presented on white background at a visual angle of 4.5° (Figure 1a).

The odor stimulus battery was derived from two base components, an oil-based peanut odorant (Peanut Flavor, Takasago International Corp., Japan) and an oil-based orange odorant (cold-pressed orange oil, Sigma Aldrich, USA). These odorants were selected to each be perceived as congruent with one of the visual stimulus categories, and incongruent with the respective other visual stimulus category. Odorants were diluted in mineral oil at concentrations that yielded iso-intense percepts, as established through pilot testing in 15 independent individuals (35% dilution for the peanut odorant, 30% dilution for the orange odorant). Using these two odorants as endpoints, an 11-step dilution series was then created ranging from 100% orange odor to 100% peanut odor in concentration steps of 10% (i.e. 90% orange, 10% peanut, 80% orange, 20% peanut etc., Figure 1b).

Task procedures

Each trial started with a black crosshair presented against a white background, which turned green to indicate imminent stimulus onset. Then, a sequence of the five images of either the ‘orange’ or the ‘peanut’ category was presented at a rate of 1 image per second. With the onset of the first image, the experimenter held a bottle containing 10 ml of an odorant up to the participant’s nostrils for 5 seconds, until the last image of the series disappeared. Odors were assigned to trials in a pseudo-randomized order and ranged between 100% image-congruency (i.e., peanut pictures/peanut odorant) to 10% image-congruency (i.e. 10% peanut in 90% orange odorant with peanut picture). Overall, the experiment consisted of 60 trials, where each individual odor-picture combination was presented 3 times. Afterwards, the question “how congruent were the odor and the picture?” was displayed on the screen. Participants registered their answer by mouse click on a visual analog scale with the anchor points “very incongruent” and “very congruent”.

Data analysis

Congruency ratings were converted to a scale from 0 (very incongruent) to 100 (very congruent). Linear effects of odor mixture levels, independent of odor type, were subsequently tested using a linear mixed effects model with “percentage of target odor in mixture” (10-100%) and “picture type” (orange vs. peanut) as fixed effects and the subject factor as a random effect.

fMRI Experiment

Participants

Twenty individuals who reported themselves as healthy and with normal olfactory and visual (correction using contact lenses allowed) functions participated in the imaging portion of the study. None of these had previously participated in the behavioral session. Two subjects were excluded for suspected malingering based on task performance, resulting in a final sample of 18 participants (11 women, M age = 28 years, SD = 7 years). Participants with metal implants, past or current neurological and psychiatric illness, self-reported smell impairment as well as current rhinitis or allergies were not recruited. Upon enrollment, all participants completed identification subtest of the Sniffin’ Sticks battery, with everyone performing above the cut-off for hyposmia (11 correct responses, Hummel, et al., 1997).

Stimuli and stimulus delivery

Based on the results from the behavioral assessment, we selected five concentrations from the 11 step dilution series based on their perceived congruency levels rather than objective mixture levels. Selected odors thus represented perceptually distinct mixture combinations (100% orange odor, 100% peanut odor, a perceptual 50/50 mixture level consisting of 40% orange and 60% peanut odor, as well

as two mixtures perceptually corresponding to 75/25% mixture levels (80% peanut, 20% orange for the peanut-dominant mix, 40% peanut, 60% orange for the orange-dominant mix). Taken together, these odors created a five-step linear dilution series ranging from a percept of 100% peanut odor to 100% orange odor. Again, participants were presented with these odors in combination with visual stimuli, and were asked to evaluate their perceived congruency. The picture battery remained identical to the behavioral assessment session.

Olfactory stimuli were presented orthonasally by means of a custom-designed, computer-controlled, 16-channel olfactometer suitable for event-related functional neuroimaging. A similar olfactometer design has been described in detail elsewhere (Lundstrom, et al., 2010). The olfactometer produces near-rectangular olfactory stimuli with fast stimulus rise time and a minimal odor concentration loss over time. In short, a valve control unit regulates the state of the olfactometer's pilot-air solenoid valves that, in turn, control the six odor-onset valves (one for each stimulus plus one for ambient air) located in close proximity to the scanner bore via individual high pressure pilot air. When an odor-onset valve is triggered, it directs a continuous airstream of 3.0 liters per minute (Lpm) into a glass reservoir containing 10 ml of the respective odorant. The odorized headspace is then transported to a birhinal nosepiece. Ambient air is automatically directed to the nosepiece in between odor presentations, serving as no-odor control airflow (0.5 Lmp). This continuous airstream masks the tactile cues that might otherwise alert the subject to channel-switching (Boesveldt, et al., 2010; Miller, et al., 2013). In the nosepiece, the flow from the activated channel (odor or control) mixes with this continuous, low-flow airstream, adding up to a total airflow of 1.75 Lpm per nostril. The time lag of odor onset was measured using a photoionization detector (Mini-PID; Aurora Inc., Ontario, Canada) and the odor triggering was adjusted

accordingly to assure synchronous onset of the odor with the visual stimuli (Lundström et al. 2010). The olfactometer was operated by trigger pulses sent through the E-Prime software package (Psychology Software Tools, Inc., Sharpsburg, PA, USA), which also controlled the projection of visual stimuli to the participants, ensuring time-locked presentations of odors and pictures, and collected the congruency ratings.

Task procedures

The experimental protocol consisted of simultaneous presentations of olfactory and visual stimuli, followed by a congruency rating task. Each trial started with the presentation of a black fixation cross, which changed to a green color for a jittered duration before stimulus presentation (1300-2100 ms) to alert participants to the imminent beginning of a new trial. This was followed by a 2000 ms presentation of a single target image (peanut or orange), as well as a simultaneously presented odor stimulus. Interspersed control trials consisted of ambient air stimulation as well as a scrambled visual stimulus as a high-level baseline.

Overall, the experiment consisted of 240 trials including 40 control trials. Of the remaining 200, 100 trials each showed orange and peanut images, of which 20 trials each were presented with an odorant corresponding to a perceived 0%, 25%, 50%, 75% and 100% perceptual overlap between the odors and visual images. Stimulus presentation was immediately followed by the question “How congruent were the odor and the picture?”. Participants were instructed to evaluate the extent to which they felt that the odorant matched the picture on the screen using an MRI-compatible button box to register their responses by moving a cursor along an 11-point visual analog scale ranging from “very incongruent (1)” to “very congruent (11)”. No congruency ratings were required for control trials. Trials where no response was given within 5000 ms were counted as non-responses. Participants were not informed how many

different odorants there were, and were encouraged to use the entire scale to provide their responses as quickly and as accurately as possible. Between trials, a black fixation cross was presented for jittered time intervals between 6000 and 9000 ms.

Data acquisition

Data were acquired on a 3T TIM Trio Siemens MRI scanner (Siemens Medical Systems, Erlangen, Germany) using a 32-channel head coil. First, structural images were acquired by means of a three-dimensional T1-weighted MPRAGE sequence (160 slices, TR: 1810 ms, TE: 3.51ms, 9° flip angle, matrix size 96x96, FOV 240x180mm^2, voxel size of 0.9x0.9x1mm$^{3)}$. Then, whole brain functional images were collected during four separate runs of 12 minutes each with a T2*-weighted interleaved EPI sequence in descending order (TR: 2500 ms, TE: 22ms, 90° flip angle, matrix size: 96x96, FOV: 240x240mm^2, voxel size: 2.5x2.5x2.5mm^3, 5mm slice gap, 40 slices). Images were acquired obliquely, at an approximate rotation of 20 degrees axial/coronal from the AC-PC line. The first three scans of each session were excluded from analysis to ensure an equilibrated MR signal.

fMRI data analyses

Preprocessing and Univariate Analysis

Data were processed using SPM8 (www.fil.ion.ucl.ac.uk/SPM) running under MATLAB R2013a (The Mathworks Inc., Sherborn, MA, USA). Images were realigned using a two-pass procedure, registering to the first image (first pass) and then the mean image (second pass), and subsequently slice-timing corrected to the last slice acquired temporally. Anatomical scans were coregistered to their respective mean EPI scans, and then normalized into standard anatomical MNI space using the nonlinear transformation matrix calculated from the mean EPI scan of each subject and the SPM

standard EPI template. Finally, functional images were smoothed with a 6mm FWHM isotropic Gaussian kernel to accommodate intersubject variations in anatomy.

Statistical analyses of the time series were performed within the framework of the General Linear Model (GLM), removing low-frequency noise with a high pass filter (128 ms cutoff period). Separate regressors for each run coded onsets of olfactory-visual stimulus presentations as events. Participant's congruency ratings were z-transformed on the subject level in an effort to adjust for potential differences in response tendencies between participants while maintaining proportional differences between conditions on the individual level. Normalized ratings were then submitted to the analysis as a parametrical modulator. Linear changes in activation (first-order modulation) as a function of these congruency ratings were assessed to determine areas where BOLD-signal was increasing or decreasing systematically with a heightened experience of perceptual overlap between the image and the odor *(integration-sensitive contrast)*. In addition, we modeled quadratic changes (second-order modulation) of stimulus-related activation by congruency: a positive U-shaped quadratic relationship would hereby indicate a maximum activation for clearly recognizable odors (i.e. 100% orange odor or 100% peanut odor, at both 0% and 100% congruency with the visual stimulus) and minimal activity for the mixed odor *(odor-object-sensitive contrast)*, while a negative U-shaped quadratic relationship would indicate maximum activity for the 50/50 odor and minimal activity when the odor is clearly congruent or clearly incongruent *(difficulty-sensitive contrast)*. While no systematic linear or quadratic effects on response time by congruency were observed behaviorally (both $p > .28$), we entered the time of button press as a linear parametric modulator of no interest to correct for potential signal variability caused by systematic differences in response duration on the MR signal. Parametric regressors were hereby

orthogonalized, so that the reaction time regressor only accounted for variance not removed by the congruency regressor. Event onsets for null events, as well as scale presentations, were modeled separately. The six realignment parameters of each scan (translations and rotations) were used as covariates of no interest to remove residual artifacts due to head movement.

Individual main contrasts of the linear and quadratic parametric modulators then entered a mixed-effects GLM for group-level inference. A random factor modeled subject-specific variance assuming unequal variances between participants. We first tested for positive and negative linear associations with congruency to identify areas characterized by gradual activations or deactivations linked to increasing perceived congruency (*integration-sensitive*). Two additional contrasts tested for either positive (*odor-object-sensitive*) or negative (*difficulty-sensitive*) quadratic effects associated with congruency ratings. For all within-subject factors, an equal variance structure was assumed.

Significant effects were visualized by extracting percent signal change from each individual's first-level peak voxel within a 10mm search volume around the group level peak, and dividing this into quantile bins for congruency ratings using the rfxplot toolbox (Gläscher 2009; Kennedy et al. 2009). All activations are reported at $p_{Peak} < .05$ family-wise error (FWE) corrected for multiple comparisons, unless otherwise noted (Penny et al. 2010). A control analysis further tested whether effects were replicated in a factorial design directly comparing effects of low to high congruency ratings, and low + high to the middle congruency ratings, respectively. This analysis yielded comparable results to the main analysis above; details can be found in the supplementary data (Supplementary Table 1 and Supplementary Figure 1).

Effective Connectivity Analysis

Next, we estimated information exchange between areas showing linear and quadratic signal change to our stimulus material using Dynamic Causal Modelling (DCM) to understand the relevance of this extended network for the formation of an integration-sensitive cortical response. As explained in further detail below, we did this by comparing various theoretically informed models that implicated the main integration-sensitive area as either a receiver of linearly modulated input (indication of integration downstream in the network) or as a receiver of external stimulation by visual input, and modulatory quadratic regulation (indicator for integration happening at this site itself).

As a first step, individual subject-level peaks were identified within a 10mm search volume around the main group level peak for each of the above contrasts. Extraction of the averaged eigenvariate time series from a 6mm sphere around this individual peak was then based on a slightly modified GLM. In this model, the regressor for valid trials from the original model was nested within an additional regressor, sensory stimulation, that coded any trial onset, including control trials. This regressor served as the driving input vector to the DCM model, based on the assumption that any anticipation of a stimulus would trigger primary sensory cortex stimulation. As in the original GLM, congruency ratings with concurrently presented odors were added as linear and quadratic parametric modulators to the valid trial regressor and described whether connections were modulated by odor identity alone (quadratic) or integrated olfactory-visual information (linear). The regressors for null events and scale presentations were omitted in this DCM-focused GLM.

A model space for connectivity patterns between these three nodes was then developed (see below for theoretical motivation). In brief, all models included the same

endogenous connection structure estimating inter- and intraregional effective connectivity, which consisted of bilateral fixed connections between all three areas (A-Matrix). Driving inputs (C-Matrix), which estimate the effect of experimental conditions on regional activity, were modeled to both the visual cortex and the olfactory cortex, accounting for the bimodal nature of the stimuli, and based on the “sensory stimulation” regressor of the GLM. Finally, bilinear, single-state deterministic DCMs with centered inputs included three classes of modulatory effective connectivity parameters (B-Matrix), which corresponded to the different forms in which the sensory information could be encoded and subsequently communicated between nodes. Given the clearly perceivable object identity of all visual stimuli, we assumed that any modulation of visual input would be binary in nature (“was an identifiable visual object presented or not?”), and thus defined it through the vector coding for any non-control trial. As explained above, olfactory object identification was hypothesized to take a quadratic shape, highest at the endpoints corresponding to 100% orange and 100% peanut odor, and was as such captured by a quadratic modulator on connections. Finally, linear modulation of a pathway, manifested by the linear parametric modulator from the GLM, would indicate its sensitivity to the integration of visual and olfactory information.

Random-effects Bayesian Model Selection (BMS) [Stephan et al., 2009] was used to rank models of the model space according to their negative free energy.

Results

Behavioral assessment

Linear mixed effects analyses demonstrated that the factor “percentage of target odor in mixture” significantly predicted the rated congruency ($b = .84$, $t(1179) = 36.59$, $p < .001$, Figure 3).

fMRI study

Behavior

The experimental modulation yielded behavioral congruency ratings from within the scanner that were strongly correlated with the established perceived levels of “percentage of target odor in mixture” based on the Behavioral assessment session ($t(3347)=55.9$, $p<.0001$), thus demonstrating the validity of the experimental manipulation (mean perceived congruency across all levels: 5.8 (SD=3.6) on 11-point scale).

fMRI – GLM

We first assessed neural areas that were sensitive to integration of the visual and olfactory information related to perceived congruence by determining linear changes in activation as a function of congruency ratings. A parametric modulation of effects that linearly correlated with the rated level of congruency *(integration-sensitive contrast)* was identified in a cluster in the right lingual gyrus, which laterally extended into the fusiform gyrus (Figure 4 and Table 1). Further, we determined the cortical areas most responsive to clearly recognizable odor objects by assessing a positive quadratic *(odor-object-sensitive)* relationship, i.e. highest signal change for clearly perceivable odors regardless of the extent of overlap with the visual stimulus. Here,

we observed a cluster covering the posterior piriform cortex and the dorsolateral amygdala bilaterally. In the left hemisphere, this cluster further extended into a second peak localized within the putamen.

Finally, we determined areas responsive to a negative quadratic *(difficulty-sensitive)* relationship, characterized by increased activity towards the most ambiguous odor mixtures, where we observed increased activity within the medial superior frontal gyrus (SFG) as well as the right middle frontal gyrus.

fMRI – Effective Connectivity

The three global peak coordinates described above (fusiform/lingual gyrus for congruency-sensitive contrast, piriform cortex for odor-object-sensitive contrast, SFG for difficulty-sensitive contrast) that showed divergent BOLD response patterns to changes in perceived congruency, formed the three nodes of our DCM analyses. Five bilinear, single-state deterministic DCMs with centered inputs formed the model space and were estimated for each subject. The goal of this analysis was to compare the evidence for the each of three nodes as a signal generator for the linear coding of sensory overlap. Given that the nodes encompassed two sensory areas and one prefrontal cortex area, we further compared the evidence for top-down modulated integration, where information between the olfactory and occipital cortices was relayed via the prefrontal cortex, and direct integration, where the prefrontal cortex area was bypassed. Taken together, these variations resulted in a model space of five models: Models 1 and 2 assumed that input from piriform to fusiform cortex would be modulated by the identity of the odor only (quadratic modulation) and subsequently integrated with visual information in fusiform cortex itself, which would thus act as the generator of the integrated signal. In Model 1, this modulation would arise directly through modulatory activity from piriform to fusiform cortex, while it would be relayed through SFG in model

2. Models 3 and 4 assumed that piriform cortex would receive image identity information in form of a binary signal modulation from fusiform gyrus; integration with olfactory information at the level of the piriform cortex would then be reflected in a linear modulation of fusiform activity. Again, in Model 3, this modulation would arise directly from piriform to fusiform cortex, while it would be relayed through SFG in Model 4. Finally, Model 5 assumed a central role of the SFG for the integration of olfactory and visual congruency, with the signal from olfactory cortex to SFG being modulated by odor object information and the signal from visual cortex to SFG being modulated by detection of a visual object. Projections from SFG to the fusiform gyrus would then be modulated in a linear manner, indicating an integration of olfactory and visual information.

The Bayesian Omnibus Risk (BOR) of the model comparison demonstrated a statistical tendency at p=0.06, indicating that no single model's probability significantly exceeded that of the others. However, to explore this pattern further, we performed Bayesian Model Averaging (BMA) (Penny et al. 2010) across all models falling within the standard Occam's window (posterior odds ratio significant at p=0.05, Madigan and Raftery, 1994). The significance of parameter estimates was established at the group level by comparing whether each posterior parameter deviated significantly from its prior (Bonferroni-corrected for multiple comparisons across all parameters). This procedure was adopted to allow for the interpretation of individual parameters across all models given the lack of evidence for one winning model. Under this approach, connections derived from more than one model can reach significance and as such, can capture an outcome where pathways from several models are simultaneously relevant (Stephan et al. 2010; Frässle et al. 2016).

Results of this procedure indicated that the pattern of significant modulation was best described as a combination of direct and top-down mediated integration, suggesting the existence of two parallel processing pathways (Figure 5). Specifically, significant averaged parameter estimates indicated a direct exchange of information between visual and olfactory cortex (input of binary visual information from visual into piriform cortex, and a linear signal indicating integration of olfactory and visual input from piriform into visual cortex, see Model 3), implicating olfactory cortex as the integration site. In parallel, we found evidence for a top-down modulated indirect route, with information being transmitted from visual cortex to SFG and on to piriform cortex, and a linear signal in return from SFG to visual cortex, implicating SFG as the integration site (see Model 5). Of interest, the quadratic modulator additionally took on a significant negative value for this connection, indicating that it was most active during conditions around the 50/50 mixture point and less active towards both the 100% and the 0% congruency point. Parameter estimates for intrinsic connectivity can be found in the supplementary data (Supplementary Figure 2).

Discussion

The aim of this study was to delineate the perceptual and cortical mechanisms that underlie the analysis of semantic object overlap across the congruency spectrum. To achieve this, we linearly manipulated perceived semantic object overlap between highly familiar visual stimuli and concurrently presented odors, while participants evaluated the extent of overlap. Our results demonstrate a linear relationship between perceived and physical overlap in stimulus properties, and thus, a fine-tuned conscious representation of variations in crossmodal overlap (Amsellem and Ohla 2016). On the cortical level, a continuous activity increase at the intersection of fusiform and lingual gyrus corresponds to the degree of perceived overlap between olfactory and visual

information. Finally, our results demonstrate that congruency-based visual-olfactory integration is mediated by two parallel pathways, characterized by a linear direct route from the olfactory to visual cortex and an indirect route linking the two sensory cortices via the SFG, which is increasingly recruited towards the middle of the congruency spectrum, where stimulus combinations are most ambiguous.

On the behavioral level, these findings thus confirm our hypothesis that humans encode overlap between concurrently perceived multisensory information in a linear manner, analogously to the encoding of typicality during object recognition based on single sensory modalities (Grill-Spector 2003; Iordan et al. 2016). In the specific case of olfactory-visual integration, this implies that, for example, during evaluation of a grocery item in the supermarket, our senses are capable of extracting not only whether the product smells “right”, given its visual experience, but also, extract an estimate of the amount of deviance from the perfect template.

Our fMRI analyses identified one principal integration-sensitive area that demonstrated a linear activation enhancement with increased congruency. This area was located occipitally in the visual cortex at the intersection of the lingual and fusiform gyri. As such, it was located in direct proximity to areas classically implicated in specialized object identification tasks, such as the lateral occipital complex (Grill-Spector et al. 2001), transverse occipital sulcus (Nasr et al. 2011) or fusiform face area (Kanwisher et al. 1997). Previous studies using a classical dichotomized congruency design have demonstrated that the fusiform gyrus is sensitive towards stimulus congruency for odor-taste (Veldhuizen et al. 2011) as well as auditory-visual combinations (Dolan et al. 2001). Our findings extend this sensitivity to semantic congruency between olfactory and visual stimuli, thus supporting the notion that the fusiform gyrus is not only a higher- order visual processing area, as traditionally

assumed, but rather, an area sensitive to the object-likeness of sensory stimuli across modalities. The linear nature of this response indicates that object representations in fusiform cortex assume a central role in the acquisition of object knowledge based on sensory pairing, and in the subsequent elicitation of flexible behavioral responses within varying environmental settings. Whether this response reflects analytical processing of crossmodal semantic overlap per se, or a more generalized response to perceptual familiarity of the object, remains to be further explored.

The precise location of the cluster within the fusiform gyrus further overlaps with activation coordinates commonly reported in studies determining neural responses to food cues, as identified through reverse inference using the online-tool Neurosynth (www.neurosynth.com). While our study did not contain any non-food stimuli and as such, any generalization needs to be approached with caution, this might indicate that, similar to other tasks of high evolutionary relevance, such as face recognition, sensory recognition of food, or visualization of food during consumption (Small et al. 1997; Gottfried et al. 2004; Lundström et al. 2008), might arise in a specific region of visual object identification cortex.

Our connectivity analyses highlight that integration of olfactory and visual information may arise as early as primary olfactory cortex. We demonstrate that this integration is communicated to fusiform cortex via both a direct and an indirect route, and that the relative significance of the two depends on task demand. These findings support the hypothesis that olfactory perception, even at an early stage, is influenced by its visual context (Jadauji et al. 2012; Qu et al. 2016). This conclusion could be perceived as being at odds with the results from the general linear model, which indicates a predominant pattern of responsiveness to odor object-likeness. Indeed, substantial experimental evidence supports the view of odor object identification as the

primary task of piriform cortex (Howard et al. 2009; Wilson and Sullivan 2011; Bekkers and Suzuki 2013). While neuroimaging results typically capture an object-dependent response, recent work suggests that piriform cortex activity might additionally be influenced by other odor object project properties, such as intensity and behavioral relevance (Wilson 2009; Roland et al. 2017). While this multidimensionality cannot be captured by a univariate analysis outcome, it can be captured by effective connectivity analyses, which model the relevance of a specific signal shape to a specific cortical connection, therefore isolating a specific neural computation from other functions of the same cortical area. We propose that the observed patterns are a reflection of such a process.

The difficulty-sensitive site in SFG, where maximal activity was detected for the 50/50 olfactory mixtures, was also most strongly connected to both olfactory and visual cortex during presentation of these ambiguous stimuli. Its location overlapped with both pre-SMA (supplementary motor area) and middle cingulate cortex, areas that are frequently being implicated in the execution of complex olfactory tasks, such as integration with other modalities (e.g. Seubert et al. 2010), or increasing stimulus complexity (Boyle, 2009). Whether this specific anatomical location is uniquely recruited in the cognitive manipulation of sensory integration remains to be explored. In combination with the concurrent inferior frontal gyrus activation, one might also integrate the overall activity pattern into the overarching concept of the multiple demand system. Coined by Duncan (Duncan 2010), this term describes a distributed activation pattern with inferior frontal and pre-SMA activation, as well as inferior parietal sulcus activation at its core. The underlying idea is that recruitment of this network is crucial to fluid intelligence and arises preferentially during the successive completion of a number of integrated tasks that might require reorganization and fluctuating

prioritization of demands. Indeed, recent work from our lab indicates that all three of these regions are robustly engaged in combination during the execution of difficult sensory integration tasks (Ohla et al. 2017; Regenbogen et al. 2017).

The observed connectivity patterns provide further insight into the functional mechanisms behind the recruitment of this network during sensory integration: rather than clearly favoring either direct low-level sensory integration or top-down mediated integration, our analyses show that both direct and prefrontally relayed integration exist in parallel, and that prefrontal mediation increases in relative importance as stimulus combinations approach an object boundary, or perceptual midpoint between two clear concepts. While perfect matches between modalities thus appear to result in direct amplification of visual cortex signal to the presented item, the zone in between, where some familiarity and some unfamiliarity can simultaneously be detected, relies on higher level cognitive processing. One potential function of this top-down control might be to provide the flexibility to move decision boundaries according to task demands or environmental contexts, a feature which is key to many forms of object perception. While our study manipulated overlap specifically for visual-olfactory stimuli, these results point to a potentially generalizable functional mechanism for processing of congruency that improves our understanding of object formation across sensory modalities. Specifically, the importance of considering intermediate perceptual steps and alternate local response patterns in the exploration of sensory integration is highlighted, given that these provide specific insight into support network recruitment during ambiguous or complex perceptual tasks. Because everyday sensory events rarely fall into the categories of completely novel or completely familiar, but rather somewhere in between, increased insight into the automatic integrative processes, but also into the integrated control function of prefrontal cortex which is executed in parallel

to ensure successful task execution, is much needed. The extent to which the precise cortical integration sites overlap between different contexts and modalities, however, remains to be further explored to provide a basis for a general understanding of human sensory integration under conditions of ambiguity. It is also important to remember that any theoretically motivated restriction of model nodes, as in DCM, represents a simplification of the actual signal transmission in the human brain. Hypothesis-free analyses of connectivity could provide a useful complement in future studies to provide both insight into possible intermediate processing steps that mediate piriform-fusiform connectivity, as well as the extended sensory and executive networks that contribute to the complex computation resulting in a linear percept of congruency.

Several limitations should be noted. One is that we did not record sniffing responses as part of our experimental paradigm. While effect sizes for modulation of piriform cortex by sniffing are usually in a smaller range than those for odor object perception (and thus would not be expected to explain the observed results in their entirety) and no link between sniff behavior and odor congruency has been demonstrated, we cannot fully rule out that participants may have adapted their sniff patterns in response to the typicality of the odor, or even to the typicality of the odor-picture combination, and that this may have had an effect on the obtained results. Moreover, congruency between the visual and olfactory stimulus may have affected the deployment of attention to the olfactory stimulus and away from the easily recognizable visual stimulus, as an adaptive mechanism to evaluate the relevance of an unexpected sensory occurrence. It should be noted, however, that there was no significant correlation between congruency and response time (, a measure that in past studies been demonstrated to be related with attentional resources allocated to the stimulus (Krupski and Boyle 1978; Carlson et al. 1983). Finally, female participants

were over-represented in our study samples, especially for the behavioral session. A number of studies indicate superior olfactory skills for women relative to men (e.g. Cain 1982), with some indication that these effects might specifically affect odors of sex-specific relevance (Pause et al. 2004; Seubert et al. 2009). Further, our recent meta-analysis of fMRI-data during olfactory tasks has revealed small, but significant sex differences across studies (Seubert et al. 2013). While these were of moderate effect sizes and not localized to the regions of interest identified in the present study, we cannot fully rule out that the observed effect sizes would be systematically affected by inclusion of a higher number of male participants.

Taken together, our results demonstrate that humans have a highly developed ability to evaluate semantic overlap between sensory modalities that extends far beyond the mere acceptance of matched stimuli and the rejection of mismatched ones. Graded perceptual evaluations directly map onto the strength of neural activity in cortical areas that are traditionally considered dedicated to visual object perception, pointing towards the inherent multimodality of these structures. The fact that cognitive control networks increasingly mediate the integration of object-relevant sensory information as percepts become more ambiguous might provide insight into flexibilities in object perception, which are essential to adaptive behavior within different environmental settings.

Acknowledgment

This work was supported by grants from the Knut and Alice Wallenberg Foundation (KAW 2012.0141 to JNL); the Swedish Research Council (2014-1346 to JNL and 2014-1384 to JS); and a DAAD postdoctoral fellowship to CR.

Bibliography

Amsellem S, Ohla K. 2016. Perceived Odor-Taste Congruence Influences Intensity and Pleasantness Differently. Chem Senses. 41:677–684.

Bekkers JM, Suzuki N. 2013. Neurons and circuits for odor processing in the piriform cortex. Trends Neurosci. 36:429–438.

Binkofski F, Buccino G, Zilles K, Fink GR. 2004. Supramodal representation of objects and actions in the human inferior temporal and ventral premotor cortex. Cortex. 40:159–161.

Cain WS. 1982. Odor identification by males and females: predictions vs performance. Chem Senses.

Corbetta M, Shulman GL. 2002. Control of goal-directed and stimulus-driven attention in the brain. Nat Rev Neurosci. 3:201–215.

Doehrmann O, Naumer MJ. 2008. Semantics and the multisensory brain: how meaning modulates processes of audio-visual integration. Brain Res. 1242:136–150.

Dolan RJ, Morris JS, de Gelder B. 2001. Crossmodal binding of fear in voice and face. Proc Natl Acad Sci USA. 98:10006–10010.

Duncan J. 2010. The multiple-demand (MD) system of the primate brain: mental programs for intelligent behaviour. Trends Cogn Sci (Regul Ed). 14:172–179.

Frässle S, Paulus FM, Krach S, Jansen A. 2016. Test-retest reliability of effective connectivity in the face perception network. Hum Brain Mapp. 37:730–744.

Gau R, Noppeney U. 2016. How prior expectations shape multisensory perception. Neuroimage. 124:876–886.

Gläscher J. 2009. Visualization of group inference data in functional neuroimaging. Neuroinformatics. 7:73–82.

Gottfried JA. 2010. Central mechanisms of odour object perception. Nat Rev Neurosci.

11:628–641.

Gottfried JA, Smith APR, Rugg MD, Dolan RJ. 2004. Remembrance of odors past: human olfactory cortex in cross-modal recognition memory. Neuron. 42:687–695.

Grill-Spector K. 2003. The neural basis of object perception. Curr Opin Neurobiol. 13:159–166.

Grill-Spector K, Kourtzi Z, Kanwisher N. 2001. The lateral occipital complex and its role in object recognition. Vision Res. 41:1409–1422.

Hebart MN, Donner TH, Haynes J-D. 2012. Human visual and parietal cortex encode visual choices independent of motor plans. Neuroimage. 63:1393–1403.

Hein G, Doehrmann O, Müller NG, Kaiser J, Muckli L, Naumer MJ. 2007. Object familiarity and semantic congruency modulate responses in cortical audiovisual integration areas. J Neurosci. 27:7881–7887.

Howard JD, Plailly J, Grueschow M, Haynes J-D, Gottfried JA. 2009. Odor quality coding and categorization in human posterior piriform cortex. Nat Neurosci. 12:932–938.

Iordan MC, Greene MR, Beck DM, Fei-Fei L. 2016. Typicality sharpens category representations in object-selective cortex. Neuroimage. 134:170–179.

Jadauji JB, Djordjevic J, Lundström JN, Pack CC. 2012. Modulation of olfactory perception by visual cortex stimulation. J Neurosci. 32:3095–3100.

Kanwisher N, McDermott J, Chun MM. 1997. The fusiform face area: a module in human extrastriate cortex specialized for face perception. J Neurosci. 17:4302–4311.

Kayser C, Shams L. 2015. Multisensory causal inference in the brain. PLoS Biol. 13:e1002075.

Kennedy DP, Gläscher J, Tyszka JM, Adolphs R. 2009. Personal space regulation by the human amygdala. Nat Neurosci. 12:1226–1227.

Kersten D, Mamassian P, Yuille A. 2004. Object perception as Bayesian inference. Annu Rev Psychol. 55:271–304.

Kersten D, Yuille A. 2003. Bayesian models of object perception. Curr Opin Neurobiol. 13:150–

158.

Kobal G, Klimek L, Wolfensberger M, Gudziol H, Temmel A, Owen CM, Seeber H, Pauli E, Hummel T. 2000. Multicenter investigation of 1,036 subjects using a standardized method for the assessment of olfactory function combining tests of odor identification, odor discrimination, and olfactory thresholds. Eur Arch Otorhinolaryngol. 257:205–211.

Landis BN, Hummel T, Hugentobler M, Giger R, Lacroix JS. 2003. Ratings of overall olfactory function. Chem Senses. 28:691–694.

Laurienti PJ, Kraft RA, Maldjian JA, Burdette JH, Wallace MT. 2004. Semantic congruence is a critical factor in multisensory behavioral performance. Exp Brain Res. 158:405–414.

Leopold DA, O'Toole AJ, Vetter T, Blanz V. 2001. Prototype-referenced shape encoding revealed by high-level aftereffects. Nat Neurosci. 4:89–94.

Lundström JN, Boyle JA, Zatorre RJ, Jones-Gotman M. 2008. Functional neuronal processing of body odors differs from that of similar common odors. Cereb Cortex. 18:1466–1474.

Lundström JN, Gordon AR, Alden EC, Boesveldt S, Albrecht J. 2010. Methods for building an inexpensive computer-controlled olfactometer for temporally-precise experiments. Int J Psychophysiol. 78:179–189.

Mesulam MM. 1998. From sensation to cognition. Brain. 121 (Pt 6):1013–1052.

Nasr S, Liu N, Devaney KJ, Yue X, Rajimehr R, Ungerleider LG, Tootell RBH. 2011. Scene-selective cortical regions in human and nonhuman primates. J Neurosci. 31:13771–13785.

Ohla K, Höchenberger R, Freiherr J, Lundström JN. 2017. Super- and subadditive neural processing of dynamic auditory-visual objects in the presence of congruent

odors. Chem Senses.

Pause BM, Ohrt A, Prehn A, Ferstl R. 2004. Positive emotional priming of facial affect perception in females is diminished by chemosensory anxiety signals. Chem Senses. 29:797–805.

Penny WD, Stephan KE, Daunizeau J, Rosa MJ, Friston KJ, Schofield TM, Leff AP. 2010. Comparing families of dynamic causal models. PLoS Comput Biol. 6:e1000709.

Pessoa L, Kastner S, Ungerleider LG. 2003. Neuroimaging studies of attention: from modulation of sensory processing to top-down control. J Neurosci. 23:3990–3998.

Qu LP, Kahnt T, Cole SM, Gottfried JA. 2016. De novo emergence of odor category representations in the human brain. J Neurosci. 36:468–478.

Regenbogen C, Axelsson J, Lasselin J, Porada DK, Sundelin T, Peter MG, Lekander M, Lundström JN, Olsson MJ. 2017. Behavioral and neural correlates to multisensory detection of sick humans. Proc Natl Acad Sci USA. 114:6400–6405.

Regenbogen C, Johansson E, Andersson P, Olsson MJ, Lundström JN. 2016. Bayesian-based integration of multisensory naturalistic perithreshold stimuli. Neuropsychologia. 88:123–130.

Rohe T, Noppeney U. 2015. Cortical hierarchies perform Bayesian causal inference in multisensory perception. PLoS Biol. 13:e1002073.

Roland B, Deneux T, Franks KM, Bathellier B, Fleischmann A. 2017. Odor identity coding by distributed ensembles of neurons in the mouse olfactory cortex. Elife. 6.

Seubert J, Freiherr J, Djordjevic J, Lundström JN. 2013. Statistical localization of human olfactory cortex. Neuroimage. 66:333–342.

Seubert J, Gregory KM, Chamberland J, Dessirier J-M, Lundström JN. 2014. Odor valence linearly modulates attractiveness, but not age assessment, of invariant facial

features in a memory-based rating task. PLoS One. 9:e98347.

Seubert J, Kellermann T, Loughead J, Boers F, Brensinger C, Schneider F, Habel U. 2010. Processing of disgusted faces is facilitated by odor primes: a functional MRI study. Neuroimage. 53:746–756.

Seubert J, Ohla K, Yokomukai Y, Kellermann T, Lundström JN. 2015. Superadditive opercular activation to food flavor is mediated by enhanced temporal and limbic coupling. Hum Brain Mapp. 36:1662–1676.

Seubert J, Rea AF, Loughead J, Habel U. 2009. Mood induction with olfactory stimuli reveals differential affective responses in males and females. Chem Senses. 34:77–84.

Small DM, Jones-Gotman M, Zatorre RJ, Petrides M, Evans AC. 1997. Flavor processing: more than the sum of its parts. Neuroreport. 8:3913–3917.

Stephan KE, Penny WD, Moran RJ, den Ouden HEM, Daunizeau J, Friston KJ. 2010. Ten simple rules for dynamic causal modeling. Neuroimage. 49:3099–3109.

van Atteveldt NM, Peterson BS, Schroeder CE. 2014. Contextual control of audiovisual integration in low-level sensory cortices. Hum Brain Mapp. 35:2394–2411.

Veldhuizen MG, Douglas D, Aschenbrenner K, Gitelman DR, Small DM. 2011. The anterior insular cortex represents breaches of taste identity expectation. J Neurosci. 31:14735–14744.

Wilson DA. 2009. Pattern separation and completion in olfaction. Ann N Y Acad Sci. 1170:306–312.

Wilson DA, Sullivan RM. 2011. Cortical processing of odor objects. Neuron. 72:506–519.

Figures

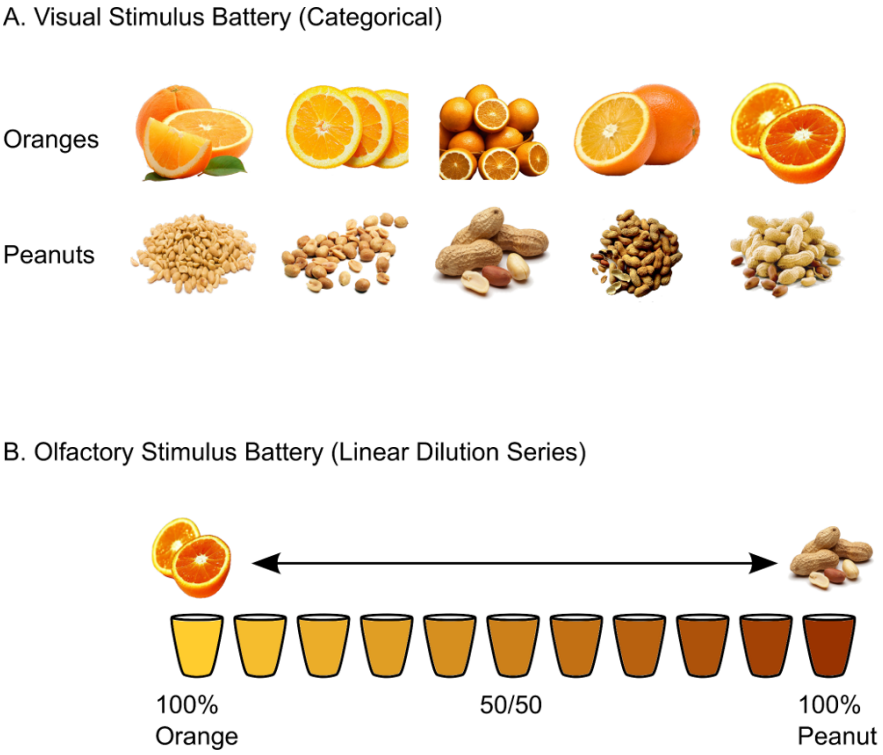

Figure 1: Stimulus batteries. A: Visual stimulus battery, oranges (top row) and peanuts (bottom row). In the Behavioral assessment session, all 5 visual stimuli were used in each trial in rapid succession, while the main experiment used one pseudo-randomly selected image per trial. **B**: Olfactory dilution series with orange odor and peanut odor as endpoints. 9 in-between steps were mixed by successive addition of peanut odor to orange odor in 10% dilution steps.

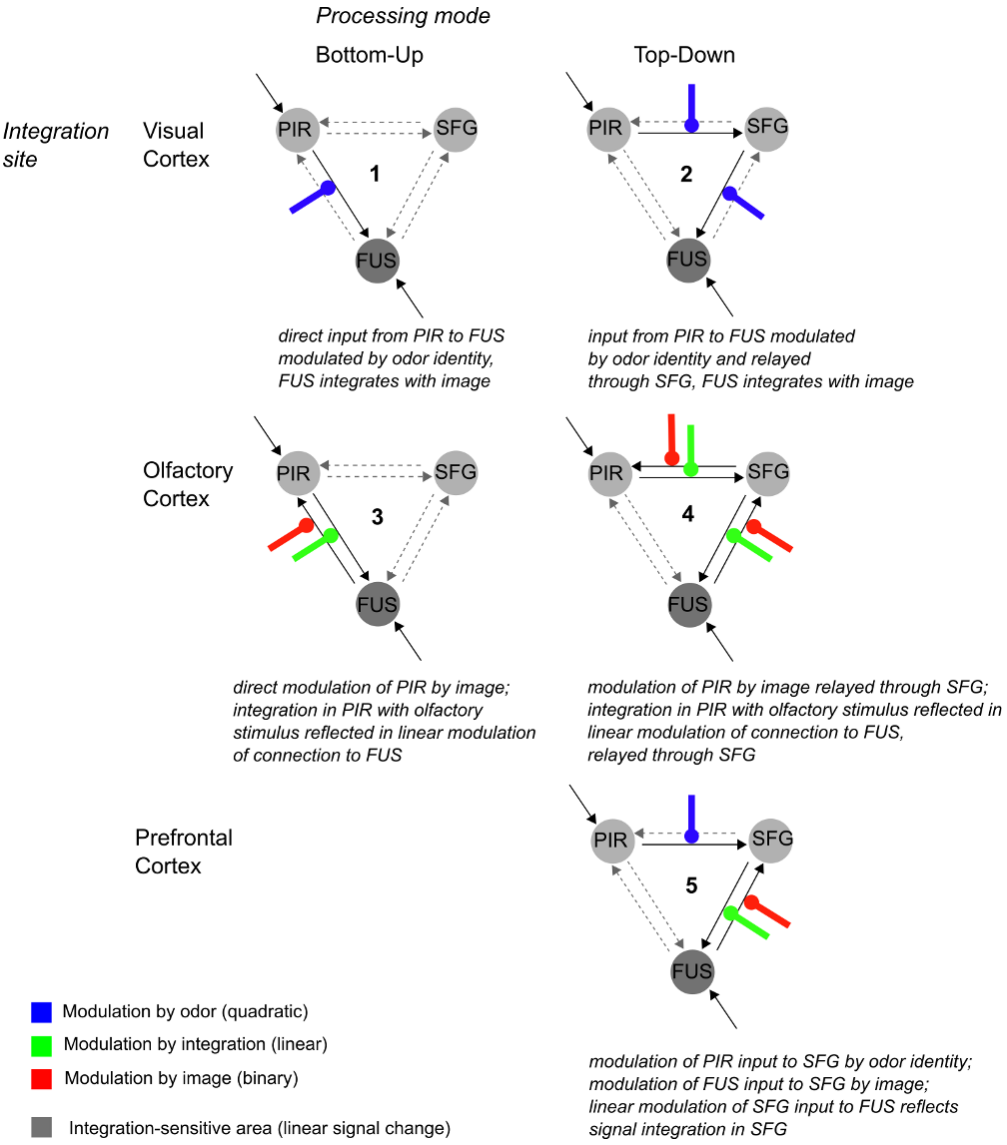

Figure 2: Model space for DCM analyses. PIR = Primary olfactory (piriform) cortex (peak from positive quadratic GLM contrast), SFG = Superior frontal gyrus (peak from negative quadratic GLM contrast), FUS = intersection of fusiform/lingual gyrus (peak from linear GLM contrast). Arrows indicate inputs and intrinsic connections; connections modulated in each of the respective models are highlighted in black. Colors of modulators indicate type of modulation for each respective model (explained further in description underneath each model).

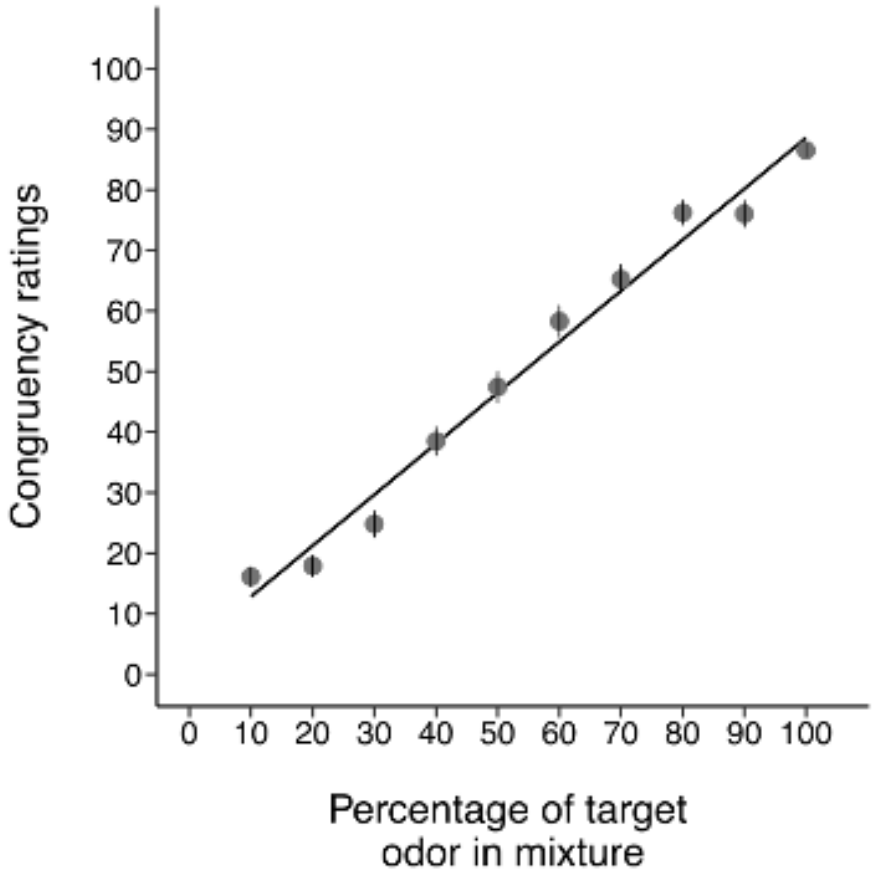

Figure 3. Perceived olfactory-visual congruency as a function of percentage of target odorant in odor mixture (+-SE). Linear fit (depicted by regression line) was significant at $p<.001$.

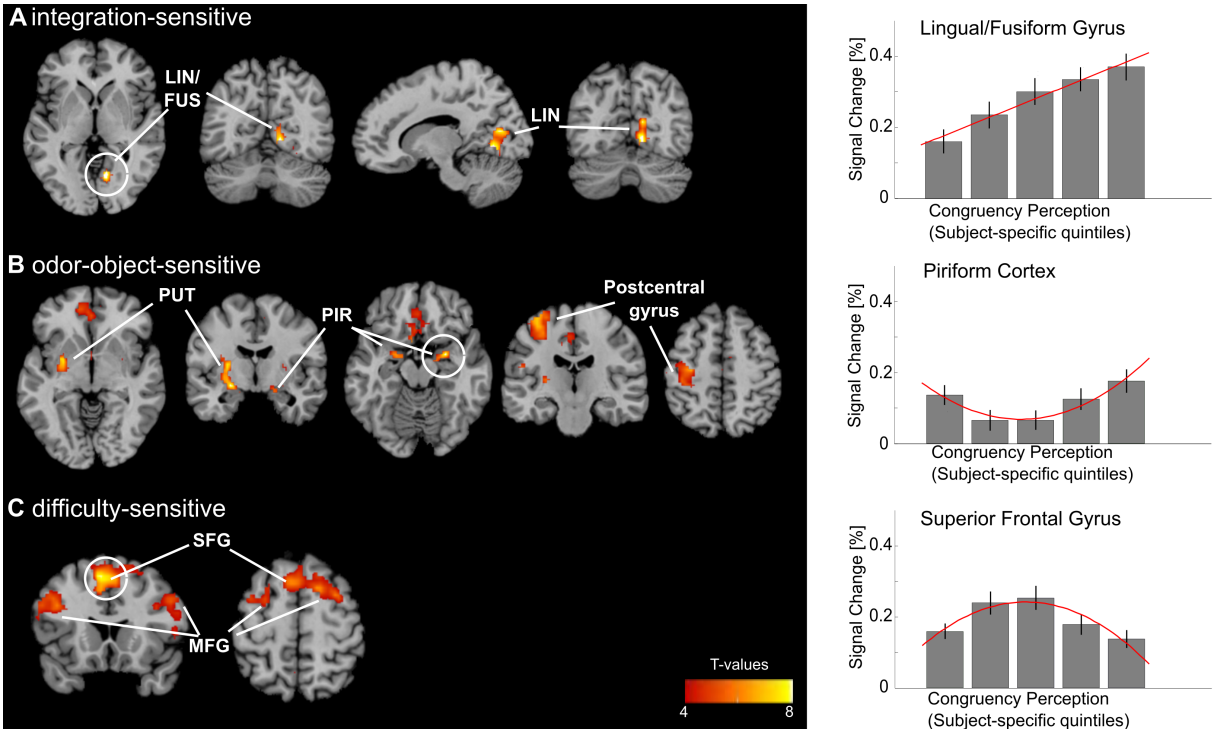

Figure 4: Whole-brain activation, as well as signal change extracted from the peak cluster (circled in white), for **A**) integration-sensitive, **B**) odor-object-sensitive, and **C**) difficulty-sensitive olfactory-visual stimulus presentations by olfactory-visual congruency (t-contrasts from a random-effects general linear model (GLM), displayed in neurological convention. For illustration purposes, clusters are depicted at a more liberal threshold (T>3.65, cluster-level corrected, p<.001). The color bar depicts t-values of local maxima peak activation. LIN = Lingual gyrus, FUS = Fusiform gyrus, PUT = Putamen, PFC = Primary olfactory (piriform) cortex, SFG = Superior frontal gyrus, MFG = Middle frontal gyrus.

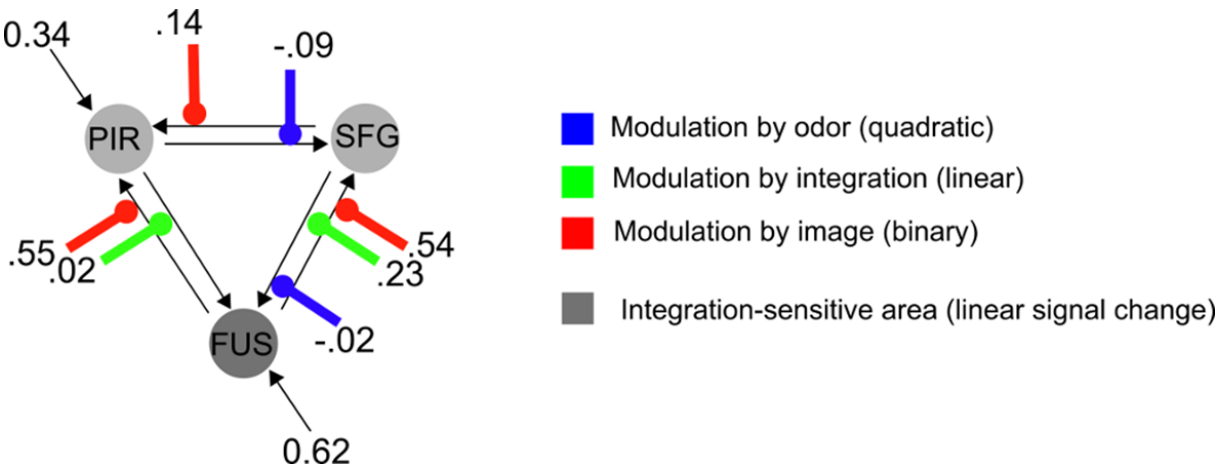

Figure 5. Results of Bayesian Parameter Averaging**.** Numbers denote group-wise average parameter estimates for respective inputs and modulations. Only parameters that were determined significant by one-sample t-test are included in the figure.

Tables

Table 1: Stereotaxic coordinates and respective neuroanatomical labels of significant local maxima of the three main contrasts.

Peak P (FWE)	Peak T	Peak Z	Cluster Size	MNI-Coordinates x	y	z	Hemis-phere	Area Label
Integration-sensitive contrast (positive linear)								
0.003	8.76	5.32	14	12	-64	-4	R	Lingual gyrus/ Fusiform gyrus
0.006	8.25	5.17	9	12	-73	11	R	Medial occipital gyrus/Lingual gyrus
Odor-object-sensitive contrast (positive quadratic)								
0.001	9.41	5.50	36	-24	-7	-13	L	Posterior piriform cortex/Dorsolateral amygdala
0.001	9.24	5.46		-24	-1	8	L	Putamen
0.003	8.76	5.32	8	27	-4	-16	R	Posterior piriform Cortex/dorsolateral amygdala
0.016	7.68	4.98	7	-36	-25	65	L	Postcentral gyrus
Difficulty-sensitive contrast (negative quadratic)								
0.010	7.97	5.08	15	-6	17	50	L	Superior frontal gyrus
0.012	7.84	5.03	7	48	38	29	R	Middle frontal gyrus

Supplementary data for the paper:

PREFRONTAL CONTROL OVER OCCIPITAL RESPONSES TO CROSSMODAL OVERLAP VARIES ACROSS THE CONGRUENCY SPECTRUM

Johan N. Lundström, Christina Regenbogen, Kathrin Ohla, and Janina Seubert

---

Table 1. Results of factorial GLM analysis comparing different combinations of the bottom third (low), middle third (middle), and top third (high) of congruency ratings (whole brain statistics for anatomical regions with significant results in main GLM analysis).

Peak P (FWE)	Peak T	Peak Z	Peak P (.001 unc)	MNI-Coordinates			Hemis-phere	Area Label
				x	y	Z		
high>low congruency ratings (integration-sensitive)								
<0.001	13.35	7.83	<.001	12	-70	2	R	Lingual gyrus/ Fusiform gyrus
high+low>middle (odor-object-sensitive)								
0.006	6.60	5.26	<.001	-21	-10	-13	L	Posterior piriform cortex/Dorsolateral amygdala
0.005	6.63	5.28	<.001	-24	-7	8	L	Putamen
>.001	8.14	6.02	<.001	30	-7	-13	R	Posterior piriform cortex/Dorsolateral amygdala
0.015	6.30	5.09	<.001	-30	-19	62	L	Postcentral gyrus
middle > high+low (difficulty-sensitive)								
0.071	5.77	4.78	>.001	-6	20	47	L	Superior frontal gyrus
0.001	7.21	5.58	>.001	-42	17	23	L	Middle frontal gyrus

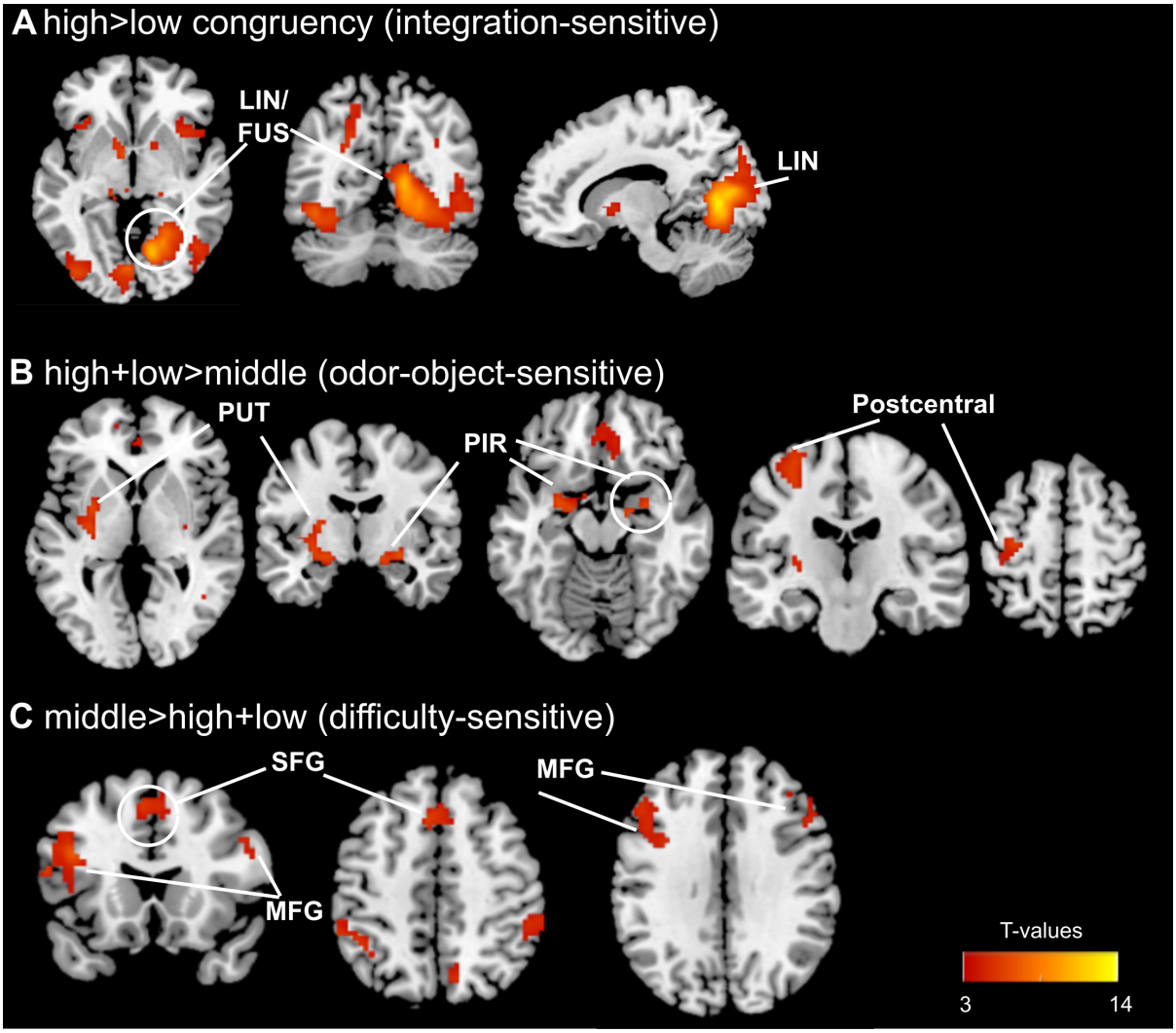

Supplementary Figure 1: Whole-brain activation from factorial GLM analysis comparing different combinations of low, middle, and high of congruency ratings. **A**) integration-sensitive (high>low), **B**) odor-sensitive (high+low>middle), and **C**) difficulty-sensitive (middle>high+low) (t-contrasts from a random-effects general linear model (GLM), displayed in neurological convention. Clusters are depicted at T>3.35, cluster-level corrected, p<.001. The color bar depicts t-values of local maxima peak activation. LIN = Lingual gyrus, FUS = Fusiform gyrus, PUT = Putamen, PFC = Primary olfactory (piriform) cortex, SFG = Superior frontal gyrus, MFG = Middle frontal gyrus.

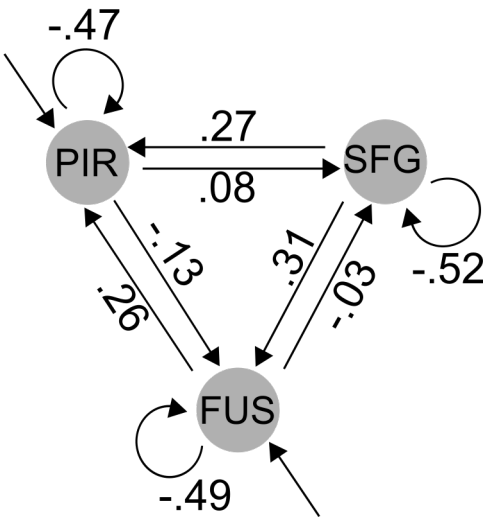

Supplementary Figure 2: Intrinsic connectivity estimates (A-Matrix) from the DCM analysis.